Rietveld refinement of the incommensurate structure of the elpasolite (ordered perovskite) Pb_2MgTeO_6

1998 J. Phys.: Condens. Matter 10 6461

(http://iopscience.iop.org/0953-8984/10/29/006)

J. Phys.: Condens. Matter **10** (1998) 6461–6472. Printed in the UK PII: S0953-8984(98)91542-9

Rietveld refinement of the incommensurate structure of the elpasolite (ordered perovskite) Pb_2MgTeO_6

G Baldinozzi†, D Grebille‡, Ph Sciau†, J-M Kiat†§, J Moret‖ and J-F Bérar¶

† Laboratoire de Chimie Physique du Solide, URA CNRS 453, Ecole Centrale de Paris, F-92295 Châtenay–Malabry Cédex, France
‡ Laboratoire CRISMAT, UMR CNRS 6058, ISMRA, F-14050 Caen Cédex, France
§ Laboratoire Léon Brillouin, CEN Saclay, F-91191 Gif-sur-Yvette Cédex, France
‖ Groupe de Dynamique des Phases Condensées, UMR CNRS 5581, Université de Montpellier 2, F-34095 Montpellier Cédex 5, France
¶ Laboratoire de Cristallographie, CNRS BP 166, F-38042 Grenoble Cédex 09, France

Received 11 February 1998, in final form 15 May 1998

Abstract. Lead magnesium tellurate, Pb_2MgTeO_6, undergoes two structural phase transitions at about 194 K and 142 K. The structures of the cubic and of the lower-temperature phase have been refined by the Rietveld method at three different temperatures (350, 220 and 6 K). The relative simplicity of the structure has allowed the incommensurately modulated structure for powder samples to be characterized. The modulated displacements of O atoms give rise to a large spread of bond lengths. Pb atoms are disordered and their average positions are away from the threefold axis. The structural resolution is compared to that from the analysis of the symmetry-adapted coordinates of the optic modes becoming totally symmetric in the lower-temperature phase.

1. Introduction

Complex lead-based ferroelectric perovskites are materials of considerable interest both from an industrial and from an academic point of view. These compounds have found application in several industrial fields as high-density capacitors, actuators, pyroelectric detectors and piezoelectric transducers (Lines and Glass 1977).

The prototype structure of perovskite compounds (ABO_3) is cubic ($Pm\bar{3}m$) and it consists of oxygen octahedra BO_6 sharing their corners and packed in a three-dimensional array while the A cations occupy the octahedral voids.

If two different species of cation, namely B′ and B″, are substituted for the B cation, the complex perovskite structure is obtained. The existence of a cationic ordering depends upon the stoichiometry, the charge and the cationic size differences. The prototype structure of compounds of general formula $A_2B'B''O_6$ exhibiting cationic ordering along ⟨111⟩ directions is called elpasolite. The space group of this structure is cubic $Fm\bar{3}m$ and a doubling of the simple perovskite cell edges occurs.

The first synthesis and characterization of powder samples of Pb_2MgTeO_6 was reported by Bayer (1963). Up to now there has been no report of successful growth of single crystals of this compound. The room temperature phase of this perovskite, Pb_2MgTeO_6, exhibits the elpasolite structure. The phase transition sequence is presented in figure 1. Dielectric

0953-8984/98/296461+12$19.50

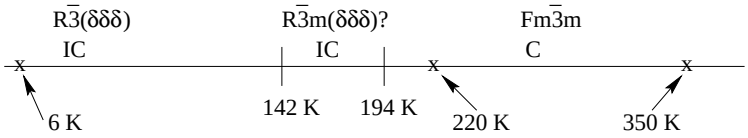

Figure 1. The phase transition sequence of Pb_2MgTeO_6; the crosses show the three data collection temperatures.

measurements performed by Politova and Venevtsev (1973) show a small anomaly in $\epsilon'(T)$ and $\epsilon''(T)$ at about 190 K. In fact, at about 194 K, the appearance of satellite reflections at incommensurate positions (Baldinozzi *et al* 1994) is the signature of a phase transition. The low-temperature phase is incommensurate with a modulation vector $(\delta\delta\delta)$ where δ is close to 0.107 at 8 K. The onset of an incommensurate phase in complex perovskites is a quite unusual phenomenon. Only three other examples have been reported: the monoclinic phases of Pb_2CoWO_6 (Tamura 1978, Sciau *et al* 1990) and of Pb_2CdWO_6 (Sciau and Grebille 1994) and possibly the trigonal phase of $PbSc_{1/2}Ta_{1/2}O_3$ (Randall *et al* 1989).

The incommensurate phase of Pb_2MgTeO_6 is particularly unusual because of its large range of existence and of the absence of lock-in. As it was already discussed in a previous paper (Baldinozzi *et al* 1994), the thermal evolution of the ferroelastic trigonal distortion let us exclude the possibility that this is the primary order parameter of the phase transition. Therefore, this phase transition is not proper ferroelastic but it is triggered by the condensation of a mode at an incommensurate point of the first Brillouin zone. The analysis of the Raman spectra gives evidence of the existence of such a soft mode, and, starting from the analysis of the compatibility relations of the two phases, the symmetry of this mode has been discussed.

The analysis of the Raman spectra and the existence of a simultaneous anomaly at 142 K in the dielectric permittivity measurements constitute evidence of a second phase transition (incommensurate–incommensurate). The symmetry of the intermediate phase can only be conjectured. On the basis of the compatibility relations of the cubic and lowest-temperature phases, the symmetry $R\bar{3}m(\delta\delta\delta)$ can be proposed. In this possible symmetry, the displacements (static and modulated) of the O atoms are much more constrained, giving a possible explanation for the pseudo-cubic features of the Raman spectra in this phase (broadening of the main peaks with no apparent splitting). Only in the lowest-temperature phase where the O atoms show the largest modulated displacements do the splitting of Raman peaks and the appearance of new Raman lines become effective: this effect can be a consequence of the symmetry lowering.

The present paper is devoted to the refinement of the structures of the cubic and the lower-temperature rhombohedral incommensurate structures. The study of the cubic phase of perovskites is not trivial (Itoh *et al* 1985, Baldinozzi *et al* 1992, Verbaere *et al* 1992, Zhukov *et al* 1995), as it has been shown that the atoms are not sited at the special positions of the prototype structure. Knowledge of the eventual disordered positions in the cubic structure is basic to the understanding of the mechanism of the phase transition.

2. Experimental procedure

2.1. Synthesis

Powdered samples of Pb_2MgTeO_6 were obtained, starting from stoichiometric amounts of high-purity PbO, TeO_2 and MgO as described in a previous paper (Baldinozzi *et al* 1994).

The x-ray diffraction pattern at room temperature shows that the powders of Pb_2MgTeO_6 obtained were well crystallized.

2.2. Data collection

Neutron diffraction patterns were collected on the 3T2 high-resolution diffractometer ($\lambda = 1.2253$ Å and $(\sin\theta_{max})/\lambda = 0.67$ Å^{-1}) at the Laboratoire Léon Brillouin in Saclay (France). Measurements were performed at 350, 220 and 6 K. The powder sample was loaded in a vanadium canister. Data collections at 350 and 220 K were performed in a flowing cryo-furnace while the 6 K recording was collected using a flowing cryostat. The thermal stability was better than 1 K. The details of the data collections are summarized in table 1.

Table 1. Characteristics of neutron data collections for Pb_2MgTeO_6.

	350 K	220 K	6 K
Wavelength (Å)	1.2253	1.2253	1.2253
Monochromator	Ge(335)	Ge(335)	Ge(335)
Step scan width 2θ (deg)	0.05	0.05	0.05
2θ-range (deg)	4.5–125.5	4.5–125.5	4.5–125.5
Monitor	30 000	30 000	40 000
Maximum counts	2201	2358	3107
Average background	69	68	72

2.3. Data analysis

The powder diffraction patterns were refined using the Rietveld program XND (version 1.16) (Bérar and Garnier 1992)†. This program has been modified to handle the refinement of incommensurately modulated phases using the de Wolff formalism (de Wolff 1977, de Wolff *et al* 1981).

During the different stages of the refinement of the modulated phase, the four-dimensional Fourier series maps were calculated using the refinement package Jana (Petříček 1994). The integrated intensities needed as input data were extracted from the powder diffraction pattern using XND.

The coefficients of the Fourier expansion of the modulation functions are used as independent parameters in the refinements: the position u_i^μ for the atom μ in the modulated structure along the coordinate axis i is given by

$$u_i^\mu(\bar{x}_4^\mu) = B_{0i}^\mu + \sum_{n=1}^{\infty}[A_{ni}^\mu \sin(2\pi n\bar{x}_4^\mu) + B_{ni}^\mu \cos(2\pi n\bar{x}_4^\mu)]$$

where $\bar{x}_4^\mu$ is the variable describing the position of the atom μ in the internal subspace defined by the modulation vector which is orthogonal to the Euclidean space ($\bar{x}_4^\mu = \boldsymbol{q}\cdot\boldsymbol{r}^\mu$, $\boldsymbol{r}^\mu$ being the average position of this atom).

The restrictions imposed by the site symmetries of the Wyckoff positions considered on the Fourier terms of the atomic modulation functions were found by solving the de Wolff equations (de Wolff 1977, de Wolff *et al* 1981). Since only first- and second-order satellites

† XND is available by anonymous ftp at ftp://labs.polycnrs-gre.fr/pub/xnd.

are observed, the refinement parameters included only Fourier amplitudes of the first and second order.

According to the *International Tables for Crystallography* (1992) the neutron scattering lengths for Pb, Te, Mg and O are 9.4017, 5.800, 5.375 and 5.803 fm respectively.

3. Results and discussion

3.1. Analysis of the cubic phase

The neutron powder diffraction patterns above the commensurate–incommensurate phase transition (194 K) can be indexed according to the face-centred cubic cell with a lattice constant of about 8 Å.

Table 2. Atomic positions in the space group $Fm\bar{3}m$.

Atom	Site symmetry	Multiplicity	x	y	z
O	$4m.m$	24	~ 0.26	0	0
Pb	$\bar{4}3m$	8	$\frac{1}{4}$	$\frac{1}{4}$	$\frac{1}{4}$
Te	$m\bar{3}m$	4	$\frac{1}{2}$	$\frac{1}{2}$	$\frac{1}{2}$
Mg	$m\bar{3}m$	4	0	0	0

In this phase, the atoms are sited at the special positions summarized in table 2. Only the O position along the Mg–Te directions and the thermal displacement factors can be refined. The site symmetry of the oxygen allows the refinement of an anisotropic thermal displacement revolution ellipsoid to be carried out. On the other hand, the lead thermal displacement ellipsoid is constrained by symmetry to be a sphere.

Table 3. Refinement results for the cubic structure (a) at 350 K and (b) at 220 K.

		(a)	(b)
a	(Å)	7.9976(5)	7.9838(5)
O	x	0.2608(1)	0.2607(1)
	u_{11} (Å^2)	0.0052(7)	0.0026(7)
	$u_{22} = u_{33}$	0.0220(3)	0.0194(3)
	B_{eq} (Å^2)	1.30	1.09
Pb	B (Å^2)	1.54(2)	1.14(2)
Te	B (Å^2)	0.50(4)	0.29(4)
Mg	B (Å^2)	0.61(4)	0.40(4)
R_{wp}		4.52	4.69
R_{exp}		2.77	2.74
S		1.63	1.71
R_F		2.57	2.59
R_I		2.35	2.12

During the different refinement stages, the oxygen stoichiometry was checked and any evidence of substitutional disorder affecting the Mg and Te atoms was tested for. No such effect was observed, as the occupancies were all equal to the nominal ones within the esd.

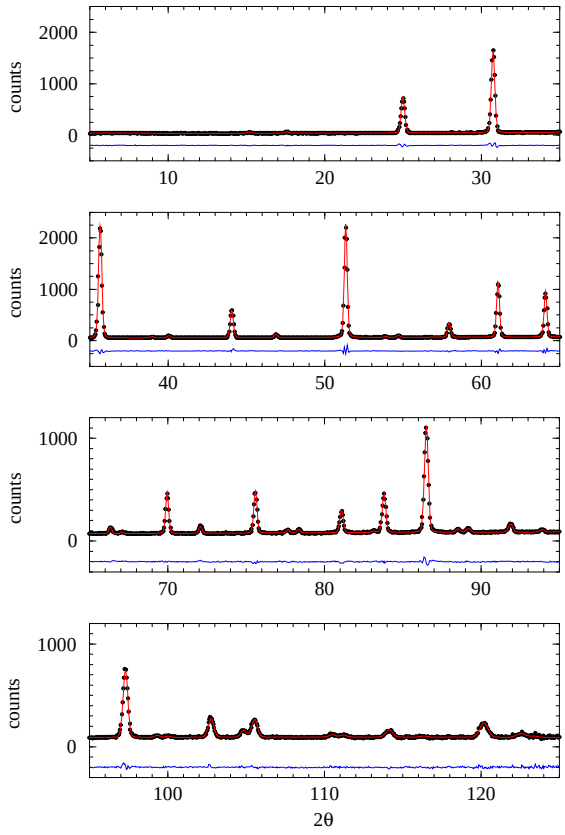

Figure 2. Neutron powder diffraction patterns of Pb_2MgTeO_6 in the cubic phase at 350 K.

The results of the final refinements at 350 and 220 K are presented in table 3. The observed, calculated and difference patterns are displayed in figure 2. The main feature of the cubic phase is the large values of the thermal factors of the lead and oxygen atoms. This can be interpreted as indicating the existence of positional disorder affecting these atoms.

It is worth noticing the singular behaviour of the coefficients describing the oxygen ellipsoid. Approaching from above the phase transition, the ellipsoid becomes more oblate: while the shorter semi-axis is divided by 2 when going from 350 to 220 K, the longer semi-axis remains unchanged. This constitutes a strong indication of an anharmonic behaviour affecting the thermal vibrations of this atom and it can be considered as a precursor phenomenon possibly related to the softening of the modes involved in the phase transition.

The situation for lead is slightly different. The thermal displacement parameter shows a significant decrease but, if a linear evolution is assumed, the intercept at 0 K is positive (about 0.45 $Å^2$).

At this point it would be interesting to perform a deeper analysis of the thermal displacement parameters like those already carried out on similar compounds (cf. Baldinozzi *et al* 1992, Vakhrushev *et al* 1994, Malibert *et al* 1997, Geddo Lehmann *et al* 1997) and split the harmonic part of the lattice vibrations from the anharmonic part related to atoms jumping back and forth between the minima of multi-well potentials.

In the present case the distance of the potential wells from the centre (estimated from the thermal displacement parameter) for lead atoms ($\boldsymbol{u}_{\mathrm{Pb}}$) is less than 0.14 Å. To quantify

the anharmonic contribution, it is necessary to span the reciprocal lattice at least up to a momentum transfer $\boldsymbol{Q}$ such that

$$\boldsymbol{Q} \cdot \boldsymbol{u}_i \approx \pi$$

where $\boldsymbol{u}_i$ is the displacement of the atom i. In the present case, for lead atoms, it would be necessary to span the Ewald sphere up to a $(\sin\theta)/\lambda$ value of about 1.8 Å^{-1}. Similar considerations apply to oxygen atoms too. This analysis is obviously not possible within the present experimental set-up.

Table 4. Bond lengths in the space group $Fm\bar{3}m$. Columns (a) and (b) report the values obtained by this structural refinement at 350 K and 220 K respectively; column (c) gives the sum of ionic radii calculated from the data in Shannon's (1976) work.

Bonding	No	(a)	(b)	(c)
Pb–O	12	2.829(1) Å	2.824(1) Å	2.84 Å
Te–O	6	1.913(1) Å	1.911(1) Å	1.91 Å
Mg–O	6	2.086(1) Å	2.081(1) Å	2.07 Å
$O–O_{Te}$	12	2.705(1) Å	2.702(1) Å	2.70 Å
$O–O_{Mg}$	12	2.950(1) Å	2.944(1) Å	2.70 Å

The bond lengths in the cubic phase at both temperatures are displayed in table 4. The calculated values are in good agreement with the values determined for similar structures and are very close to the sums of the ionic radii, supporting the proposal of ionic character for the bondings. It is interesting to note that the strong anisotropic character of the O thermal displacement can be also modelled as a libration of oxygen octahedra. In this case, we can expect the bonding lengths B–O to be slightly longer.

3.2. Analysis of the incommensurate phase

The onset of the incommensurate modulated phase, characterized by the appearance of satellite reflections, is also accompanied by a very small trigonal distortion.

Table 5. Modulated atomic displacements allowed in the space group $R\bar{3}m(\delta\delta\delta)$.

Atom	B_0	A_1	B_1	A_2	B_2
O	$x = y, z$	$A_{1x} = A_{1y}$, A_{1z}	$B_{1x} = B_{1y}$, B_{1z}	$A_{2x} = A_{2y}$, A_{2z}	$B_{2x} = B_{2y}$, B_{2z}
Pb	$x = y = z = \frac{1}{4}$	$A_{1x} = A_{1y} = A_{1z}$	$B_{1x} = B_{1y} = B_{1z}$	—	—
Te	$x = y = z = \frac{1}{2}$	$A_{1x} = A_{1y} = A_{1z}$	$B_{1x} = B_{1y} = B_{1z} = 0$	—	—
Mg	$x = y = z = 0$	$A_{1x} = A_{1y} = A_{1z}$	$B_{1x} = B_{1y} = B_{1z} = 0$	—	—

According to electron microscopy, x-ray diffraction, dielectric and polarization measurements (Baldinozzi *et al* 1997), two centrosymmetric trigonal space groups, $R\bar{3}m$ and the subgroup $R\bar{3}$, can be proposed. The modulated phase is mono-incommensurate and all order satellites can be indexed according to the modulation vector $\boldsymbol{q} = \delta\boldsymbol{a}^\star + \delta\boldsymbol{b}^\star + \delta\boldsymbol{c}^\star$, $\delta \approx \frac{1}{9}$ (Baldinozzi *et al* 1994). The refinement of the structure at 6 K in the $R\bar{3}m$ space group, where oxygen atoms are constrained to be sited on a mirror plane (cf. table 5), is not fully satisfactory ($R_{wp} = 7.73\%$, $R_{Iall} = 7.52\%$).

Moreover, the large value of the thermal displacement parameter of lead (0.74 Å^2) led us to suppose that this atom is not sited at the special position. The modulated displacements (necessarily along the threefold axis) do not help in reducing the thermal factor and suggest the existence of displacive disordered positions away from the symmetry axis. This *static* residual component of the thermal displacement parameter is even larger than the predicted value obtained by interpolating the two determinations for the cubic phase. The situation is rather similar for oxygen, where the symmetry requires the average position to be sited in the mirror planes while the refinement suggests the main components of the modulated displacements to be normal to these.

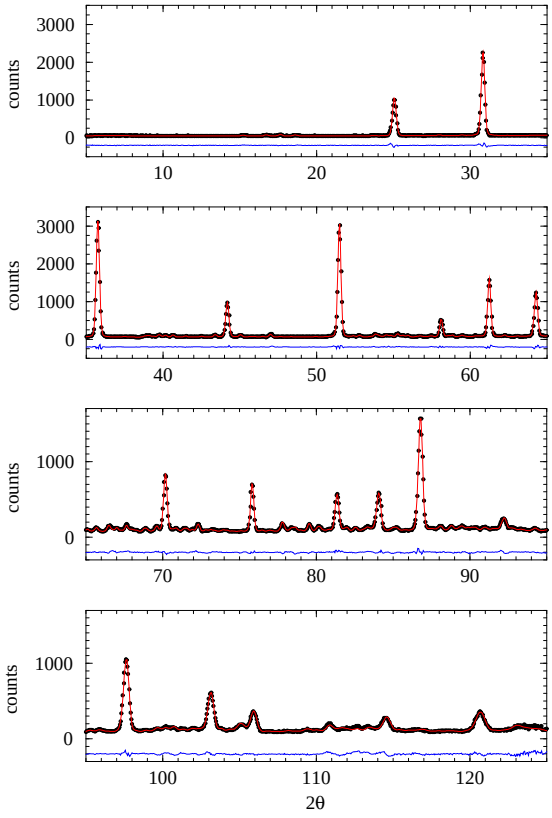

Figure 3. Neutron powder diffraction patterns of Pb_2MgTeO_6 in the incommensurately modulated phase at 6 K.

These are the main reasons that have led us to consider the subgroup $R\bar{3}$, where some more degrees of freedom are allowed for the description of the O atom. Nevertheless, within this group lead atoms still appear to be constrained too much when sited on the threefold axis at $(\frac{1}{4}\frac{1}{4}\frac{1}{4})$. Therefore this constraint was relaxed, allowing disordered positions for Pb. Two different models were checked: Pb sited on the threefold axis at (xxx) and away from the axis at a general position. Within this latter model, a significant improvement of the refinement is obtained with a very limited increase of the number of independent parameters (cf. table 5). The final result is presented in table 6. The observed, calculated and difference patterns are displayed in figures 3 and 4. Low R-factors are obtained for satellites of all orders (table 7).

To avoid the strong correlations between the thermal and the modulated displacements, some of these parameters were constrained; moreover, the terms representing meaningless

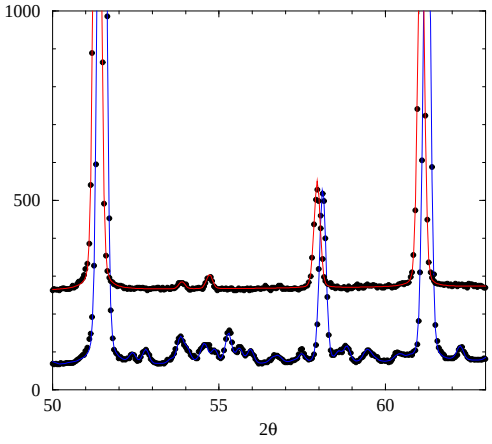

Figure 4. Detail of the refinement (experimental and fitted profile) of the neutron powder diffraction pattern of Pb_2MgTeO_6 in the incommensurately modulated phase at 6 K and in the cubic phase at 350 K. The cubic pattern has been shifted upward for clarity.

Table 6. Atomic positions and isotropic thermal parameters in the incommensurate structure at 6 K ($a = 5.6447(5)$ Å, $\alpha = 59.923(4)^\circ$, $\delta = 0.1066(3)$). The parameters marked with †, ‡ or ♯ are constrained. Some terms (⋆), allowed by the symmetry constraints, were forced to 0 as the correlations with the other structural parameters were too strong.

Atom		B_0	A_1	B_1	A_2	B_2
O	x	0.2408(6)	−0.0412(6)	−0.0234(6)	0.0072(12)	−0.0167(9)
	y	−0.2616(5)	0.0416(5)	−0.0017(10)	−0.0036(12)	0.0138(8)
	z	−0.2441(6)	−0.0099(5)	0.0018(10)	0.0102(9)	−0.0099(10)
	B	0.05(2)†				
Pb	x	0.248(4)	−0.010(6)	⋆		
	y	0.224(4)	0.018(5)	⋆		
	z	0.274(2)	−0.003(3)	0.0217(6)		
	B	0.05(2)†				
Te	x		−0.0006(4)‡			
	y		−0.0006(4)‡			
	z		−0.0006(4)‡			
	B	0.49(4)				
Mg	x		0.0013(4)♯			
	y		0.0013(4)♯			
	z		0.0013(4)♯			
	B	0.05(2)†				

Table 7. Refinement statistics: incommensurate structure.

	6 K
R_{wp}	5.07
R_{exp}	2.37
S	2.14
R_{F0}	2.65
R_{F1}	7.25
R_{F2}	7.84
R_{Iall}	4.53

shifts from the null value were also set to zero. This procedure has led us to refine a common thermal displacement parameter for all atoms except Te, which exhibits a larger

value needing some further discussion (see below).

The analysis of the compatibility relationships between the cubic and trigonal phases indicates that the modes belonging to the four irreducible representations (IR) become totally symmetrical in the low-temperature phase. Therefore, they can possibly play a role in the $Fm\bar{3}m \longrightarrow R\bar{3}$ phase transition. Two of these IR are at the zone centre (T_{1g} and T_{2g}); the others are at the $\boldsymbol{q}$-point (Λ_1 and Λ_2) (Baldinozzi *et al* 1997) belonging to the Λ line.

The modulated structure exhibits large modulated displacements for O atoms. These displacements are well described by the Raman mode Λ_2. These displacements are mainly transverse to the modulation vector (and almost along $[1\bar{1}0]_c$). Nevertheless, the longitudinal components cannot be neglected in the actual structural refinement (as $T \ll T_c$).

Table 8. Bondings: incommensurate structure.

Bonding	No	Mean	Standard deviation	Minimum	Maximum
Pb–O	12	2.831 Å	±0.172 Å	2.409 Å	3.236 Å
Te–O	2 × 3	1.983 Å	±0.091 Å	1.833 Å	2.106 Å
Mg–O	2 × 3	2.029 Å	±0.088 Å	1.910 Å	2.172 Å
O–O	12	2.835 Å	±0.222 Å	2.452 Å	3.262 Å

On the other hand, Pb atoms are at rest in the mode Λ_2 (Baldinozzi *et al* 1997). Therefore the modulated displacements for this cation are probably related to another mode triggered by the condensation of Λ_2. This is possibly the case for the modes belonging to the T_{2g} irreducible representation. In these modes, associated with the ferroelastic distortion which acts as a secondary order parameter, the Pb atoms vibrate along $[100]_c$ directions. Since this zone-centre optic mode is threefold degenerate in the cubic phase, linear combinations of the displacements are also possible, and the resulting displacement of the Pb atoms can be quite complex. Moreover, the superposition of these displacements and the static disorder (Pb atoms are not sited on the threefold axis) increases the complexity of this description. This complex picture is well reflected by the large dispersion of the 12 Pb–O bond lengths displayed in table 8.

The remaining atoms in the structure (Te and Mg) are weakly modulated. The modulation is symmetry constrained to be longitudinal as they are sited on the threefold axis. The amplitudes are quite small and, as the modulated displacements respect the Λ_1 symmetry, they may be associated with a residual displacement related to the existence of the commensurate–incommensurate phase transition ($Fm\bar{3}m \longrightarrow R\bar{3}m(\delta\delta\delta)$) for which the order parameter is supposed to have this symmetry.

The effect of these modulated displacements, especially for the heavier atoms in the structure, has been checked for coherence with an x-ray diffraction pattern at the same temperature. In this pattern, almost no satellite peak is observed with a standard recording time. The x-ray pattern calculated using the neutron structure confirms the absence of strong satellites and supports the existence of a displacive disorder affecting Pb atoms. The main contribution to satellite peaks in fact comes from O displacements.

These modulated displacements give rise to the bond distances displayed in figures 5, 6 and 7. The average bond lengths for the incommensurate phase (table 8) are almost the same as those already observed for the cubic phase. In some regions of the crystal, three short Pb–O bonds of length less than 2.6 Å may occur. The large modulated displacements of O atoms are responsible for the large dispersion of the bond lengths around these average values, giving rise to some short O–O bonds. These deformations induce an averaging of the effective sizes of the two types of octahedron. This result can be explained if the modulated

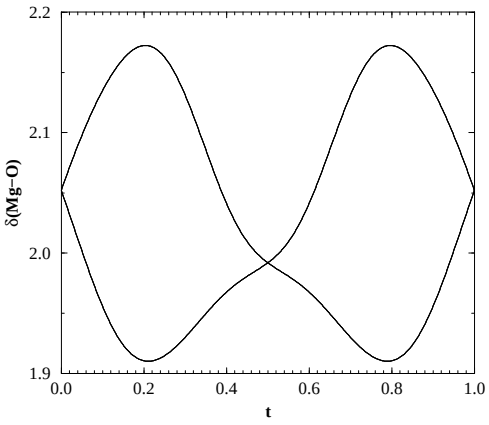

Figure 5. Mg–O distances in the modulated structure ($t = x_4 - \boldsymbol{q} \cdot \boldsymbol{r}$). Each one of the two sets of distances is representative of the bondings of Mg with the three O atoms defining the two octahedron faces normal to the threefold axis.

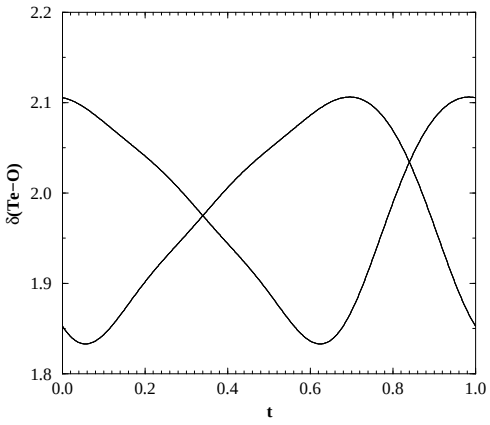

Figure 6. Te–O distances in the modulated structure.

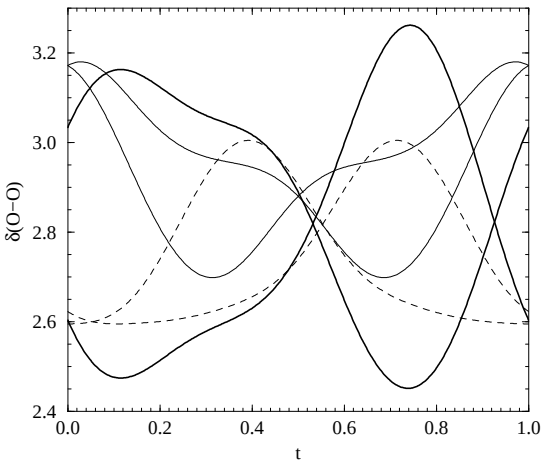

Figure 7. O–O distances in the modulated structure. The bold solid lines represent the lengths of the bonds between atoms belonging to the same octahedron face normal to the threefold axis. The other lines refer to the bonds between atoms belonging to the remaining octahedron faces.

displacements are poorly modelled using a Fourier development based on sinusoidal waves: a more accurate description would be obtained by including crenel-like functions. The physical counterpart of this description is a crystal in which weakly modulated regions are separated by anti-phase boundaries.

A particular feature that needs further discussion is represented by the large thermal displacement parameter of the Te atom (it is larger in the incommensurate phase than in the cubic phase). This is possibly related to the breaking of the regular stacking of large and small octahedra characteristic of the $Fm\bar{3}m$ cubic lattice. The modulation wave defines a structure in which there is no longer a direct relationship between the size of the octahedra in the layer and the atom sited at the octahedra centre. As there is only one independent O atom in the structure, the relative distortion is more important for the smaller octahedron. Therefore, the environment of Te is more affected and this is responsible for the *artificial* increase of the thermal displacement parameter of the Te atom.

4. Conclusion

The cubic structure of Pb_2MgTeO_6 is very close to the prototype elpasolite one. No compositional disorder is observed for Te and Mg. In this structure, the thermal displacement parameters for Pb and O atoms are quite large: in particular, the O thermal motion is strongly anisotropic.

Below 194 K, the structure is incommensurately modulated and the compound undergoes a second phase transition (incommensurate–incommensurate) at about 140 K. The structure of the lower-temperature phase has been determined at 6 K. The analysis of the modulated displacements suggests that the primary order parameter of the second phase transition belongs to the Λ_2 irreducible representation (Baldinozzi *et al* 1997). On the other hand, Pb atoms are disordered and their average positions lie away from the threefold axis. The modulated displacements affecting Pb atoms are quite complex, but they are probably compatible with a linear combination of the modulated displacements described by the T_{2g} modes. The ferroelastic trigonal deformation which exhibits the behaviour of a secondary order parameter actually belongs to this representation (Baldinozzi *et al* 1994).

These modulated displacements, and in particular those related to O atoms, give rise to a large range of bond lengths. This dispersion can be actually observed in the crystal or simply be the result of the smoothing of a crystal structure in which anti-phase boundaries separate weakly modulated regions. EXAFS experiments could establish which one of the two hypotheses is the most accurate. In fact, if the modulated displacements are well described within the sinusoidal approximation, no signal should be observed, because of the dispersion of the bond lengths. On the other hand, a sharp signal should be obtained if the modulated displacements are well described with a crenel function.

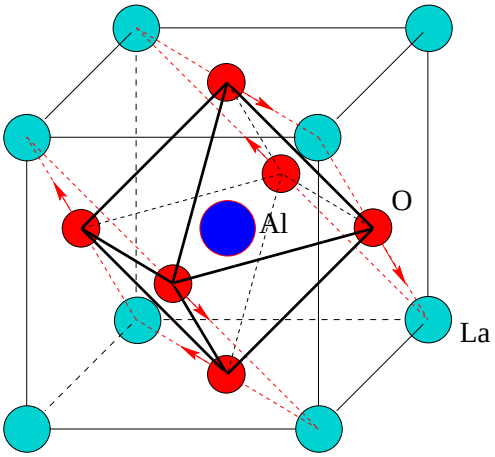

Figure 8. Atomic displacements of the soft mode responsible for the $LaAlO_3$ phase transition. In Pb_2MgTeO_6 the displacements of the upper and lower octahedron faces associated with the soft Λ_2 mode are independent. This feature is responsible of the inequivalence of the B–O bonds (2×3 distances)

It is instructive to compare the phase transition mechanism for Pb_2MgTeO_6 to those for other perovskite compounds exhibiting a trigonal phase at low temperature. For the rare-earth aluminates (e.g. $LaAlO_3$) (Scott 1974), a phase transition from a cubic ($Pm\bar{3}m$) to a trigonal phase ($R\bar{3}c$) is observed. An optic phonon of T_{2u} symmetry goes soft at

the [111] corner of the Brillouin zone. Since this optic mode is threefold degenerate in the cubic phase, linear combinations of the displacements are possible. These can correspond to rotation-like distortions of the octahedra about [100] as in $SrTiO_3$ giving rise to the tetragonal distortion, about [111] as in $LaAlO_3$ where the distortion is trigonal, or about [110] where the orthorhombic distortion does not minimize the free energy (Thomas and Müller 1968) and the resulting lattice is thermodynamically unstable; therefore this structure is not actually observed. In this case, the octahedra distort in a way that can be approximated by a rigid rotation about the threefold axis [111] (figure 8). Actually, this is not a true rotation, as the O atoms remain on the cube faces and, therefore, the B–O distance increases.

This picture of the phase transition is rather similar to what happens for Pb_2MgTeO_6. In the present case, the mode softening takes place at $\boldsymbol{q}$ along the Λ line. As in the rare-earth aluminates, this mode involves only O displacements along $[1\bar{1}0]_c$ directions, but it cannot be approximated by a rigid rotation about the threefold axis [111] as the displacements of the O atoms belonging to the two opposite octahedron faces normal to [111] are independent. This particular feature gives rise to two sets of three B–O bond lengths as displayed in figure 5 and figure 6.

The primary component of the displacements in the incommensurate phase behaves as the displacements described with Λ_2. This does not exclude the possibility of the existence of secondary components for atomic shifts. Nevertheless, in our opinion, these components are related not to the driving process leading to the phase transition, but to secondary order parameters such as the coupling with the strain.

References

Baldinozzi G, Sciau Ph and Bulou A 1997 *J. Phys.: Condens. Matter* **9** 10 531

Baldinozzi G, Sciau Ph and Lapasset J 1992 *Phys. Status Solidi* a **133** 17

Baldinozzi G, Sciau Ph, Moret J and Buffat P A 1994 *Solid State Commun.* **89** 441

Bayer G 1963 *J. Am. Ceram. Soc.* **46** 604

Bérar J F and Garnier P 1992 *2nd APD Conf.* NIST Special Publication, vol 846 (Washington, DC: US Government Printing Office) p 212

de Wolff P M 1977 *Acta Crystallogr.* A **33** 493

de Wolff P M, Janssen T and Janner A 1981 *Acta Crystallogr.* A **37** 625

Geddo Lehmann A, Kubel F and Schmid H 1997 *J. Phys.: Condens. Matter* **9** 8201

International Tables for Crystallography 1992 vol C, ed A J C Wilson (Dordrecht: Kluwer) section 4.4.4

Itoh K, Zeng L Z, Nakamura E and Mishima N 1985 *Ferroelectric.* **63** 29

Lines M E and Glass A M 1977 *Principles and Applications of Ferroelectric and Related Materials* (Oxford: Clarendon)

Malibert C, Dkhil B, Kiat J-M, Durand D, Bérar J-F and Spasojevic de Biré A 1997 *J. Phys.: Condens. Matter* **9** 7485

Petříček V 1994 *Jana '94 Crystallographic Computing System* Institute of Physics, Academy of Sciences of the Czech Republic, Prague

Politova E D and Venevtsev Yu N 1973 *Dokl. Acad. Nauk* **209** 838

Randall C A, Markgraf S A, Bhalla A S and Baba-Kishi K 1989 *Phys. Rev.* B **40+41** 413

Sciau Ph and Grebille D 1994 *Aperiodic '94; Proc. Int. Conf. on Aperiodic Crystals* (Singapore: World Scientific) pp 460–4

Sciau Ph, Krusche K, Buffat P A and Schmid H 1990 *Ferroelectricity* **107** 235

Scott J F 1974 *Rev. Mod. Phys.* **46** 74

Shannon R D 1976 *Acta Crystallogr.* A **32** 751

Tamura H 1978 *Ferroelectricity* **21** 449

Thomas H and Müller K A 1968 *Phys. Rev. Lett.* **21** 1256

Vakhrushev S, Zhukov S, Fetisov G and Chernishev V 1994 *J. Phys.: Condens. Matter* **6** 4021

Verbaere A, Piffard Y, Ye Z G and Husson E 1992 *Mater. Res. Bull.* **27** 1227

Zhukov S G, Chernishev V V, Aslanov L A, Vakhrushev S and Schenk H 1995 *J. Appl. Crystallogr.* **28** 385